Kinetics of PIP_2 metabolism and KCNQ2/3 channel regulation studied with a voltage-sensitive phosphatase in living cells

Björn H. Falkenburger, Jill B. Jensen, and Bertil Hille

Department of Physiology and Biophysics, University of Washington, Seattle, WA 98195

The signaling phosphoinositide phosphatidylinositol 4,5-bisphosphate (PIP_2) is synthesized in two steps from phosphatidylinositol by lipid kinases. It then interacts with KCNQ channels and with pleckstrin homology (PH) domains among many other physiological protein targets. We measured and developed a quantitative description of these metabolic and protein interaction steps by perturbing the PIP_2 pool with a voltage-sensitive phosphatase (VSP). VSP can remove the 5-phosphate of PIP_2 with a time constant of τ <300 ms and fully inhibits KCNQ currents in a similar time. PIP_2 was then resynthesized from phosphatidylinositol 4-phosphate (PIP) quickly, τ = 11 s. In contrast, resynthesis of PIP_2 after activation of phospholipase C by muscarinic receptors took ~130 s. These kinetic experiments showed that (1) PIP_2 activation of KCNQ channels obeys a cooperative square law, (2) the PIP_2 residence time on channels is <10 ms and the exchange time on PH domains is similarly fast, and (3) the step synthesizing PIP_2 by PIP 5-kinase is fast and limited primarily by a step(s) that replenishes the pool of plasma membrane PI(4)P. We extend the kinetic model for signaling from M_1 muscarinic receptors, presented in our companion paper in this issue (Falkenburger et al. 2010. *J. Gen. Physiol.* doi:10.1085/jgp.200910344), with this new information on PIP_2 synthesis and KCNQ interaction.

The Journal of General Physiology

INTRODUCTION

Phosphoinositides are minority phospholipids of biological membranes that are central in cellular signaling and as anchors for peripheral membrane proteins (e.g., De Matteis and Godi, 2004; Wenk and De Camilli, 2004). The phosphoinositide phosphatidylinositol 4,5-bisphosphate (PIP_2), localized mainly in the cytoplasmic leaflet of the plasma membrane, is required for function of many ion channels and transporters (Hilgemann and Ball, 1996; Hilgemann et al., 2001; Suh and Hille, 2002, 2008). It is also important in exocytosis, endocytosis, cell adhesion, and motility (e.g., Di Paolo and De Camilli, 2006; Mao and Yin, 2007). Additionally, PIP_2 is the immediate precursor for three major second messengers, inositol 1,4,5-trisphosphate (IP_3), diacylglycerol (DAG), and phosphatidylinositol 3,4,5-trisphosphate, which are generated by activation of plasma membrane receptors. Here, we determine the kinetics of production of PIP_2 and its regulation of KCNQ2/3 (Kv7.2/7.3) potassium channels.

We have previously investigated signaling to KCNQ channels by the M_1 muscarinic receptor (M_1R). These studies established the requirements (Suh et al., 2004; Horowitz et al., 2005), timing (Jensen et al., 2009), and rate constants (see Falkenburger et al. in this issue) of individual steps in the M_1R signaling cascade: the binding of the muscarinic agonist oxotremorine-M (Oxo-M), the processing of G proteins on receptors, G protein dissociation/rearrangement, the binding of $G\alpha_q$ subunits to PLC, and PLC-mediated hydrolysis of PIP_2. The PIP_2 depletion turns off KCNQ2/3 potassium channels (diagramed in Fig. 1, A and B).

Recovery of current after M_1R activation requires regeneration of PIP_2. Wortmannin sensitivity and an ATP requirement implicate a type III phosphatidylinositol (PI) 4-kinase in the recovery (Suh and Hille, 2002; Zhang et al., 2003). The PI 4-kinases phosphorylate PI at the inositol 4 position to produce PI(4)P, which is then phosphorylated by phosphatidylinositol 4-phosphate (PIP) 5-kinases at the 5 position to yield PIP_2 (Fig. 1 E). These two steps are required for the maintenance of the "hormone-sensitive" pool of PIP_2 at the plasma membrane (Nakanishi et al., 1995; Wang et al., 2004) and for its recovery after receptor activation.

Here, we seek a quantitative description of the lipid kinases and phosphatases that govern plasma membrane PIP_2. Most interesting is PIP 5-kinase, the enzyme producing PIP_2, which also mediates the effects of Rho family GTPases on actin organization (Chong et al., 1994;

Correspondence to Bertil Hille: hille@u.washington.edu

Abbreviations used in this paper: CFP, cyan fluorescent protein; Ci-VSP, voltage-sensitive phosphatase from *Ciona intestinalis*; DAG, diacylglycerol; Dr-VSP, voltage-sensitive phosphatase from *Danio rerio*; FRET, Förster resonance energy transfer; IP_3, inositol 1,4,5-trisphosphate; IRES, internal ribosome entry site; M_1R, M_1 muscarinic receptor; Oxo-M, oxotremorine-M; PH, pleckstrin homology; PI, phosphatidylinositol; PIP, phosphatidylinositol 4-phosphate; PIP_2, phosphatidylinositol 4,5-bisphosphate; VSP, voltage-sensitive phosphatase; YFP, yellow fluorescent protein.

The Rockefeller University Press $30.00
J. Gen. Physiol. Vol. 135 No. 2 99–114
www.jgp.org/cgi/doi/10.1085/jgp.200910345

Oude Weernink et al., 2004). To perturb the system, we characterized and exploited a PIP_2 5-phosphatase that can be activated by depolarization of the membrane potential, the voltage-sensitive phosphatase (VSP). VSP contains a voltage sensor domain homologous to those of voltage-gated ion channels and a phosphatase domain homologous to PTEN, a polyphosphoinositide phosphatase (Fig. 1, C and D) (Okamura et al., 2009). VSP can dephosphorylate PI(4,5)P_2 to PI(4)P (Iwasaki et al., 2008; Halaszovich et al., 2009). Recovery after VSP activation is then mediated by the endogenous PIP 5-kinases at the plasma membrane. As VSP-induced changes in PIP_2 were not accompanied by the generation of other second messengers that might modulate KCNQ2/3 current, this intervention also provided an opportunity to learn more about the interaction of PIP_2 with KCNQ2/3 channels, and about PIP_2 reporting by the pleckstrin homology (PH) domain probe we use.

MATERIALS AND METHODS

Cell culture and plasmids

Cells (tsA201) cultured in DMEM (Invitrogen) with 10% serum and 2% penicillin/streptomycin were passaged once a week. Cells were transfected at 75% confluency, plated on polylysine-coated glass chips 24 h after transfection, and used for experiments the next day. Cells were transfected with Lipofectamine 2000 (10 µl for a 3-cm dish; Invitrogen) and 0.5–1.2 µg DNA per plasmid: mouse M_1R (provided by N. Nathanson, University of Washington, Seattle, WA); human eCFP-PH(PLCδ1) and eYFP-PH(PLCδ1; provided by K. Jalink, The Netherlands Cancer Institute, Amsterdam, Netherlands); human KCNQ2 and rat KCNQ3 (provided by D. McKinnon, State University of New York, Stony Brook, NY); PIP 5-kinase type Iγ (provided by Y. Aikawa and T.F. Martin, University of Wisconsin, Madison, WI); and Ci-VSP-IRES-GFP (Ci-VSP, VSP from *Ciona intestinalis*; internal ribosome reentry site [IRES]) and Dr-VSP-IRES-GFP (Dr-VSP) from zebrafish (*Danio rerio*; both provided by Y. Okamura, Osaka University, Osaka, Japan). "Dark" Dr-VSP (without IRES-GFP) was generated by subcloning the Dr-VSP cassette into pcDNA3.0 using HindIII and XhoI.

Electrophysiology

Cells were continuously superfused with Ringer's solution containing (in mM): 160 NaCl, 2.5 KCl, 2 $CaCl_2$, 1 $MgCl_2$, 10 HEPES, and 8 glucose, pH 7.4 (NaOH). 10 µM Oxo-M was applied via a two-barrel theta tube. Cells were recorded by whole cell gigaseal voltage clamp using borosilicate glass pipettes with a resistance of 1.6–2.2 MΩ. Internal solution was (in mM): 175 KCl, 5 $MgCl_2$, 5 HEPES, 0.1 K_4BAPTA, 3 Na_2ATP, and 0.1 Na_3GTP, pH 7.4 (KOH). Recordings used an EPC9 amplifier with either Patchmaster 2.35 or Pulse 8.53 software (HEKA). Holding potential was −60 mV. Voltage protocols are given in the figures and legends. Currents were filtered at 2.9 kHz. Sample intervals ranged from 0.1 ms for tail currents to 50 ms for 30-s records at −20 mV. Series resistance was compensated by 70% after compensation of fast and slow capacitance. Except where stated, leak was not subtracted. For measuring VSP "sensing currents," we changed three conditions: the internal solution was (in mM) 100 HEPES, 65 NMDG, 3 $MgCl_2$, and 1 EGTA; the external solution was (in mM) 180 HEPES, 75 NMDG, 1 $CaCl_2$, 1 $MgCl_2$, and 10 glucose, pH 7.4 (as in Hossain et al., 2008); and linear leak and capacitive transients were subtracted by a p/5 procedure (five repetitions of 0.2 of the test pulse amplitude from a holding potential of −120 mV after the test pulse).

KCNQ2/3 current was measured in two ways. One was to hold the membrane potential at −20 mV continuously. Endogenous currents in tsA201 cells are small at −20 mV (−26 pA ± 5 pA; n = 16 cells; see Fig. S2, A and C). The second method used tail currents. Every 0.5 or 1 s, the membrane potential was depolarized to −20 mV for 200 or 300 ms and repolarized to −60 mV. KCNQ2/3 current activates slowly upon depolarization and deactivates slowly upon repolarization (see Fig. S2 B). In contrast, endogenous currents deactivate too fast to be seen at the sampling frequency used. KCNQ2/3 tail currents were measured by comparing current at 20 and 200 ms after repolarization to −60 mV.

Photometric measurement of PH domain Förster resonance energy transfer (FRET)

We used epifluorescence photometry to measure the FRET of PH domains simultaneously with measurement of KCNQ2/3 current. The photometry setup was different from that used previously (Jensen et al., 2009; Falkenburger et al., 2010). A monochromator (Polychrome IV; TILL Photonics) provided excitation light, and a three-color dichroic mirror in the microscope reflected at 440, 500, and 580 nm (CFP, YFP, and mCherry; 89006bs; Chroma Technology Corp.). The dichroic mirror is transparent at 460–480 and 520–560 nm. Fluorescence was detected by a photometry system consisting of a ViewFinderIII with two photodiodes connected to an FDU-2 detection unit (TILL Photonics). Light was split between the two photodiodes by a dichroic mirror (DCLP505). In addition, the short-wavelength channel contained a D480/40 emission filter, and the long-wavelength channel contained an ET535/30 filter (Chroma Technology Corp.). For near-simultaneous acquisition of CFP_C (440-nm excitation and 480-nm emission), YFP_C (440-nm excitation and 535-nm emission), and YFP_Y (500-nm excitation and 535-nm emission), the excitation wavelength was scanned from 300 to 500 nm in 200 ms. Both photodiodes were sampled every 0.1 ms. A shutter was opened 10 ms before scanning and closed 100 ms after scanning. To measure KCNQ2/3 current at the same time, the membrane potential was depolarized to −20 mV for 300 ms and held at −60 mV for the remainder of the time. This protocol was repeated every 500 ms. After recording from each cell, an area of the coverslip without cells was measured as background. This background fluorescence was small and depended little on the excitation wavelength. The light intensity in the illuminated 139 × 158.5 μm^2 area was 45 µW at 430 nm and 35 µW at 500 nm (∼0.2 W/cm^2).

Data were analyzed offline in IGOR Pro 6.0 (WaveMetrics). To calculate FRET, we extracted three values from each wavelength scan, similar to a three-cube FRET approach. We denote them CFP_C, raw YFP_C, and YFP_Y, with the first part referring to the emission wavelength and the subscript referring to the excitation wavelength. For the CFP_C value, emission in the short-wavelength channel (460–480-nm emission) was integrated over the time when excitation was 360–460 nm. For the raw YFP_C value, the long-wavelength channel (535/30-nm emission) was integrated over the same time. For the YFP_Y value, the long-wavelength channel was integrated over the time where excitation was 490–500 nm. The units for all three values were set as arbitrary fluorescence units (AFU). Background was subtracted from each. The raw YFP_C value had to be corrected for cyan fluorescent protein (CFP) emission collected in the long-wavelength channel and for direct excitation of yellow fluorescent protein (YFP) by 440-nm light by subtracting 0.834*CFP_C and 0.065*YFP_Y. The corrected value is referred to as YFP_C from now on. The correction factors were determined by measuring cells expressing only CFP or YFP. The spectral window for collection of CFP emission was smaller than

in our previous work (Jensen et al., 2009). Therefore CFP_C had to be multiplied by a larger factor in correcting the long-wavelength channel for bleedthrough of CFP emission. The lower values for CFP_C also affected the values of the FRET ratio, FRETr (see below). FRET was expressed as the ratio $FRETr = YFP_C/CFP_C$. This ratio is related to FRET efficiency, with two differences. A FRET efficiency of 20% means that 20% of CFP excitation is reemitted by YFP instead of CFP, thus CFP emission is reduced to 80%. If the short-wavelength detector (CFP_C) and the long-wavelength detector (YFP_C and YFP_Y) had the same photon sensitivity, a FRET efficiency of 20% would correspond to a FRETr of 20/80 = 0.25. However, in the photometry setup used here, the absolute changes in YFP_C were approximately threefold larger than the accompanying changes in CFP_C (both in ΔAFU; compare Fig. 2, D with E). A true FRET efficiency of 20% would therefore correspond to a FRETr of 3*20/80 = 0.75. We report FRETr in arbitrary units because the absolute values will differ between setups.

The YFP_Y value should be unaffected by FRET. It showed a gradual decline over time, reflecting dialysis of the PH probes from the cell into the much larger patch pipette. The time constant of decline (~5 min) was similar to that for CFP protein diffusing from the patch pipette into the cell. The same decline was seen in the CFP_C channel. Finally, as a consequence of the increasing distance between donors and acceptors, their FRET interaction also showed some decline.

Modeling

A kinetic model of phosphoinositide metabolism was formulated as a compartmental model in the Virtual Cell framework (University of Connecticut). The Virtual Cell Model "Falkenburger JGP2010" is publicly available at http://www.vcell.org/ under shared models/hillelab.

Statistics

Summarized data include one data point per cell. Bars and markers represent mean ± SEM.

Online supplemental material

Fig. S1 shows VSP-sensing currents in tsA201 cells. Fig. S2 illustrates endogenous ion currents in tsA cells compared with currents in KCNQ2/3-transfected cells. Fig. S3 shows the theoretical prediction of the density of PH probes at the membrane for different amounts of PIP_2, and a description of the dependence of FRET efficiency and FRETr for CFP/YFP-labeled PH probes on plasma membrane PIP_2. Table S1 lists the model differential equations. The online supplemental material is available at http://www.jgp.org/cgi/content/full/jgp.200910345/DC1.

RESULTS

Our laboratory has already formulated a preliminary kinetic description of the signaling steps from muscarinic receptor excitation to PIP_2 turnover and channel modulation (Suh et al., 2004). It was based on plausible estimates knowing the final modulation of KCNQ2/3 channels. Then, a second-generation model for the steps from receptor activation to turning on PLC was formulated in our companion paper (Falkenburger et al., 2010) based on our recent more complete set of kinetic measurements with FRET (Jensen et al., 2009). In this paper, to extend our model to include the steps of PIP_2 metabolism and the action of PIP_2 on channels, we have made extensive use of PH domains as indicators of PIP_2, of a VSP to deplete PIP_2 rapidly, and of KCNQ2/3 channels to report their own activation by PIP_2. We start by characterizing VSP.

The voltage sensor of VSP responds rapidly

As in voltage-gated ion channels, positive charges in the S4 segment of the voltage sensor of VSP (Fig. 1, C and D,

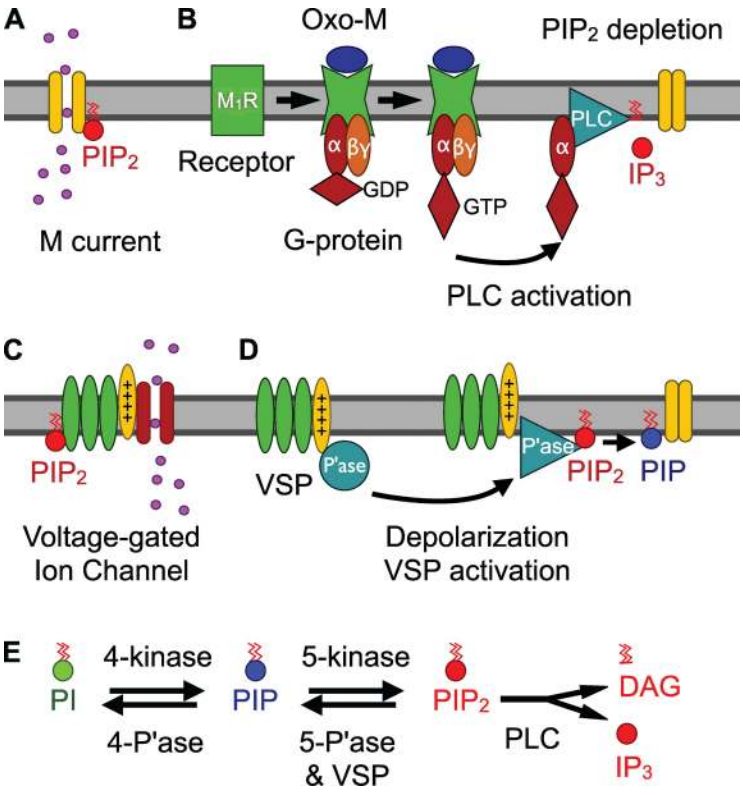

Figure 1. M_1R signaling and phosphoinositide metabolism. (A) Neuronal M current is mediated by KCNQ2/3 potassium channels (yellow), which require membrane depolarization and PIP_2 to open. (B) Binding of the M_1R agonist Oxo-M facilitates binding of G proteins to the receptor. This binding induces "activation" of G proteins, i.e., nucleotide exchange at the $G\alpha_q$ subunit from GDP to GTP, and dissociation of $G\alpha_q$ from $G\beta\gamma$. $G\alpha_q$-GTP activates PLC, which cleaves PIP_2 into DAG and IP_3. The absence of PIP_2 prevents KCNQ2/3 channels from opening. (C) Voltage-gated ion channels are tetramers. Each subunit consists of a four-segment (S1-S4) voltage sensor domain (green and yellow) and a pore-forming domain (dark red). The S4 segment (yellow) contains positive charges, which move upon depolarization. (D) VSPs are monomers. They contain a four-segment voltage sensor and a phosphatase domain. The phosphatase is activated by depolarization and dephosphorylates PIP_2 to PI(4)P. (E) Phosphoinositide metabolism. PI is phosphorylated first by a PI 4-kinase and then by a PIP 5-kinase to yield $PI(4,5)P_2$. A 4-phosphatase and a 5-phosphatase mediate the reverse reactions. VSP is a 5-phosphatase.

yellow) move outward upon depolarization, making a transient outward current, termed "gating current" for ion channels and "sensing current" for this nonchannel enzyme. The charge movement leads to activation of the phosphatase activity (Murata et al., 2005; Murata and Okamura, 2007). We determined the voltage dependence of the charge movement and its time course for VSP from zebrafish (Dr-VSP) and *Ciona* (Ci-VSP) expressed in tsA201 cells (Fig. S1). Depolarization for 100 ms elicited an outward sensing current, and repolarization elicited an inward current. The integrals over both segments were equal and represent the total charge moved during voltage sensing. At +100 mV with Dr-VSP, for example, the exponential time constant of decay of the major sensing current was $\tau = 39 \pm 4$ ms ($n = 4$ cells), and on return to −60 mV, the return charge flowed with time constant $\tau = 8.6 \pm 1.1$ ms ($n = 5$ cells), in full agreement with Hossain et al. (2008). We did not attempt to resolve additional slow time constants reported by others (Villalba-Galea et al., 2008). For Dr-VSP, the voltage dependence of this sensing charge (the Q-V curve) followed a Boltzmann relation, with a midpoint at +100 mV and a slope factor of 1.5 elementary charges. From this, Dr-VSP would be inactive at −20 mV, where we measure KCNQ current. A depolarization to +100 mV moves 50% of VSP-sensing charge and is well tolerated by our cells. By comparison, the voltage dependence of Ci-VSP was left-shifted and less steep. These findings agree with previous measurements of VSP-sensing currents (Hossain et al., 2008). To ensure that VSP remained inactive at −20 mV in our experiments, we subsequently used only Dr-VSP.

Total sensing charge also provides an estimate of the density of VSP molecules in transfected cells. The VSP construct we used included GFP after an IRES, so transfected cells would likely express more copies of VSP than of GFP. We chose cells by their visible GFP fluorescence, but unlike the previous papers (Jensen et al., 2009; Falkenburger et al., 2010), we did not quantitate this fluorescence by photon counting. In the group of cells chosen, the saturating charge movement was 4.9 ± 1.9 pC for Dr-VSP– and 2.1 ± 0.8 pC for Ci-VSP–transfected cells (five and three cells). These numbers are similar to those obtained by the Okamura group in the same cell type (4.6 pC for Dr-VSP and 5.2 pC for Ci-VSP; Hossain et al., 2008). This charge corresponds to around 20,000 and 9,000 elementary charges moved per μm^2 of plasma membrane (assuming 15 pF of cell capacitance and 1,500 μm^2 of cell surface; Falkenburger et al., 2010). The slope of the voltage dependence suggests that 1.5 charges move per voltage sensor, indicating around 13,000 expressed Dr-VSP or 6,000 Ci-VSP molecules per μm^2. The density of Dr-VSP is thus two- to fourfold higher than that of fluorescent signaling proteins determined in our companion paper (Falkenburger et al., 2010). Of note, the VSP density is also a little higher than the concentration that we chose for its substrate PIP_2 in our model.

Others have made kinetic models of the conformational changes of VSP, combining observations of charge movement and of signals from various attached fluorescent labels (Villalba-Galea et al., 2008; Akemann et al., 2009). They include fast conformational changes and sometimes several slower steps. The constructs they studied had the phosphatase enzyme mutated to be inactive or entirely deleted and sometimes replaced by one or two fluorescent proteins. None of these models gives direct information about how soon the phosphatase activity is turned on after the initial major charge movement occurs. However, our experiments below suggest that the enzyme activity is nearly synchronous with or follows charge movements within tens of milliseconds. For simplicity, we refer to our standard +100-mV depolarizations as "VSP activation."

Activation of VSP reduces PIP_2 and KCNQ2/3 current

We now use VSP activation to perturb the endogenous plasma membrane PIP_2 pool. To measure PIP_2 depletion during VSP activation, we used FRET between two fluorescently labeled PH domains from PLCδ1 (PH-CFP and PH-YFP) as described previously (van der Wal et al., 2001; Jensen et al., 2009). PH probe FRET reports PIP_2 surface density because binding to PIP_2 at the plasma membrane brings the CFP and YFP close enough together for FRET to occur. FRET between these probes decreases as PIP_2 is depleted and increases as PIP_2 recovers (Fig. 2, A–C, and Materials and methods). To calculate FRET, we measured three values (CFP_C, raw YFP_C, and YFP_Y) during VSP activation, made corrections, and calculated the FRET ratio $FRETr = YFP_C/CFP_C$ as described in Materials and methods. Upon activation of VSP by depolarization to +100 mV for 2 s, PIP_2 was depleted, and we observed (1) an increase in CFP_C fluorescence (Fig. 2 D), (2) a decrease in YFP_C fluorescence (Fig. 2 E), (3) little change in YFP_Y fluorescence (Fig. 2 F), and (4) a strong reversible drop in FRETr (Fig. 2 G). FRETr fell almost to zero during VSP activation, suggesting that much of PIP_2 was lost in that time. The mean ON time constant of the VSP-induced depletion was 421 ms at +100 mV, and the mean recovery time constant after repolarization was 6.5 s at −60 mV (Fig. 2, I and J). Thus, in a few hundred milliseconds we could convert most of the membrane PIP_2 to PI(4)P, and in 10–20 s the PIP_2 was restored.

The relationship between membrane PIP_2 and PIP_2-sensitive KCNQ current was revealed by coexpressing KCNQ2/3 potassium channels with VSP. Initially, KCNQ2/3 current was measured by the tail current amplitude (see Materials and methods). The fluorescence and current traces in Fig. 2 (D–H) were recorded simultaneously during depletion of PIP_2. Activation of VSP decreased the KCNQ2/3 tail current quickly (Fig. 2 H),

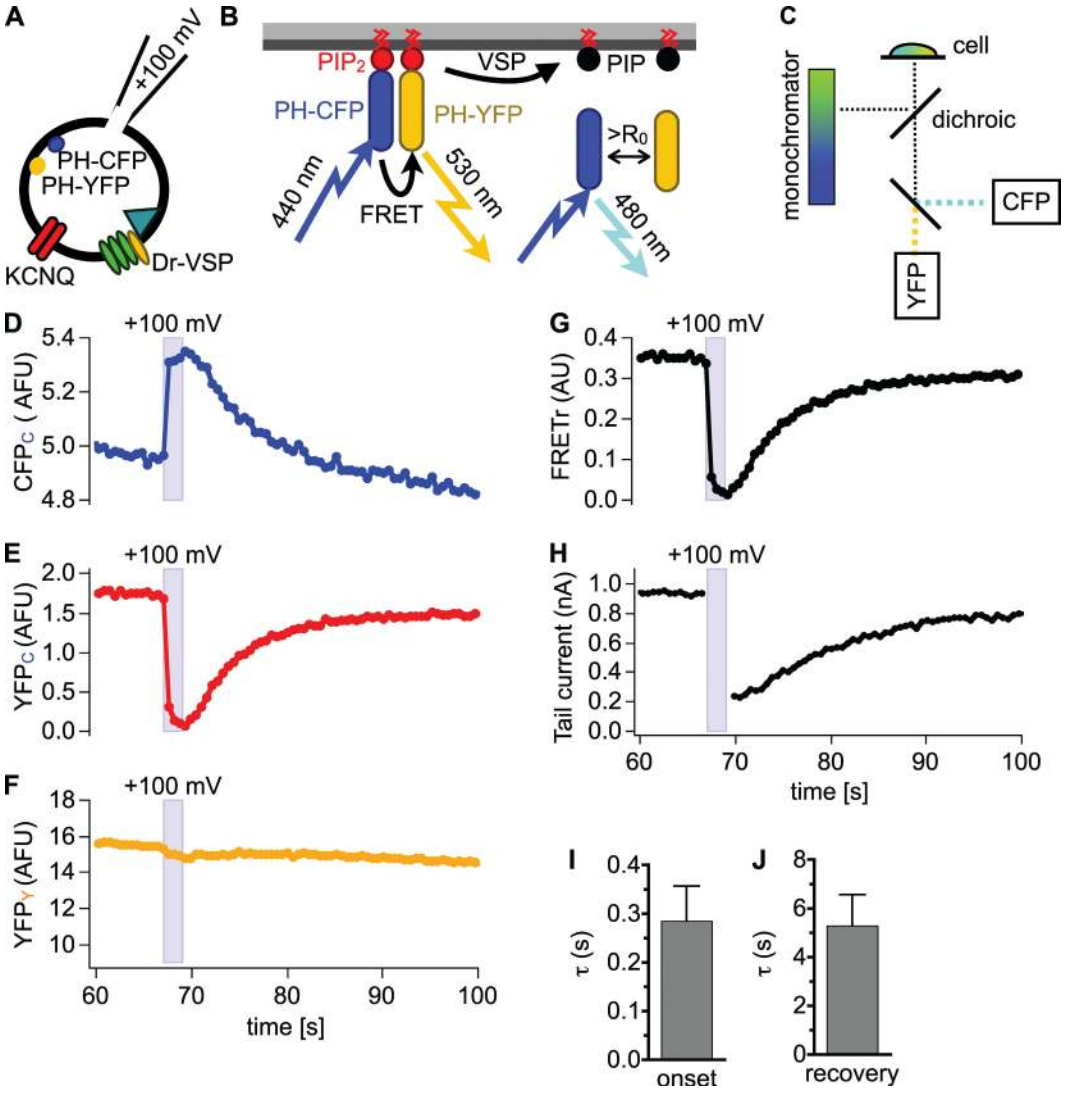

Figure 2. Activation of VSP (Dr-VSP) reduces PH probe FRET. (A) Cells were transfected with PIP_2-binding PH probes (PH-PLCδ1) fused to CFP or YFP, Dr-VSP, and KCNQ2 and KCNQ3 channel subunits and recorded in whole cell voltage clamp. (B) Principle of PIP_2 measurement by PH probe FRET (see Results and Fig. S3). (C) Photometry setup. Excitation light was scanned from 300 to 500 nm in 200 ms, every 500 ms, and reflected by a dichroic mirror around 440 and 500 nm. Emission light was separated into channels for CFP emission (480/40 nm) and YFP emission (535/30 nm). Time courses (D, E, F, and H) were acquired simultaneously. (D) CFP emission with 440-nm excitation (CFP_C). (E) YFP emission with 440-nm excitation, corrected for CFP emission at 535/30 nm and for direct excitation of YFP by 440-nm excitation light (YFP_C). (F) YFP emission with 500-nm excitation (YFP_Y). (G) FRETr = YFP_C/CFP_C. (H) Tail current amplitude. Membrane was held at −60 mV and depolarized to −20 mV for 300 ms every 500 ms, except for shaded area where membrane was held at +100 mV for 2 s. Tail currents were measured during slow channel deactivation at −60 mV. (I) Time constants of single-exponential fits to FRETr while membrane was held at +100 mV (onset of VSP effect). A summary of 14 cells is shown. (J) Time constant of single-exponential fits to recovery of FRETr after 2 s at +100 mV. A summary of 12 cells is shown.

as reported previously (Murata and Okamura, 2007). When VSP was turned off again, the recovery of current was slower than recovery of PH probe FRETr (compare Fig. 2, H with G).

To quantitate the kinetics of VSP actions on KCNQ2/3 current, we switched to measuring current by holding continuously at −20 mV, where noninactivating KCNQ2/3 current can be maintained for a long time and other endogenous K^+ currents in tsA201 cells are minimally activated (Fig. S2, A and D). PH probes were not expressed in these experiments. VSP was activated by brief steps to +100 mV, a perturbation that also increased the driving force for K^+ and, in cells without VSP, increased current through KCNQ2/3 and endogenous channels (Fig. 3 A). When Dr-VSP was coexpressed (Fig. 3 B), KCNQ2/3 current decayed during the +100-mV depolarization. Current was much reduced upon return to −20 mV and recovered thereafter. We compared currents at −20 mV before and after varying lengths of VSP activation to track the onset of the VSP effect (Fig. 3, C and D). The effect on KCNQ2/3 was maximal after a 1-s activation pulse. A half-maximal effect required

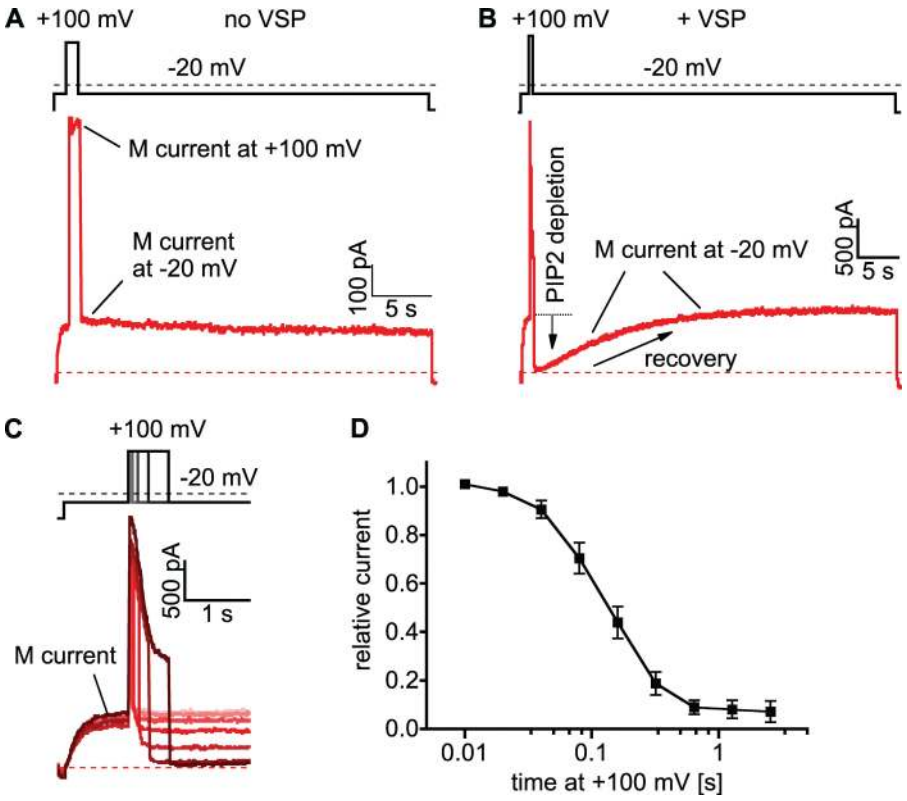

Figure 3. Activation of VSP (Dr-VSP) inhibits KCNQ2/3 current. (A) Currents recorded in cells transfected with KCNQ2/3 alone. (B) Currents in cells transfected with KCNQ2/3 and Dr-VSP. Note the reduction of current at −20 mV after depolarization to +100 mV. (C) Responses in the same cell as in B to a family of stimuli with increasing duration at +100 mV. Magnified time scale as compared with B also shows reduction of current at +100 mV. (D) Summary of normalized outward current at −20 mV (after/before step to +100 mV) for different durations at +100 mV (note log scale of x axis) for 5–12 cells.

~120 ms, and significant effect was already evident with only 40 ms of VSP activation, just enough time for 63% movement of the voltage sensor charge (Fig. S1 A). Thus, the coupling of the VSP voltage sensor to the phosphatase activity and the reporting of PIP_2 depletion by KCNQ2/3 current are both fast (<40 ms). Fitting exponentials to the decline of whole cell current at +100 mV (Fig. 4 A) gave a time course for the action of VSP consistent with that of Fig. 3 D, even though this measure would be contaminated by the slow activation of KCNQ2/3 current and the inactivation of endogenous currents at +100 mV (Fig. S2, A and B).

KCNQ2/3 current is proportional to the square of PH domain FRET

Now we can consider the relationship between PIP_2 and current. During and after VSP activation, the changes of KCNQ2/3 current and those of the PH domain FRETr were not linearly related to each other. First, their exponential time constants differed systematically. For the onset of inhibition, current decayed faster than FRET, whereas for the recovery, current returned more slowly than FRETr (Fig. 4, A and B). The recovery of current followed an S-shaped time course (Figs. 2 H, 3 B, and 4 C), and when current was plotted against FRETr, the relationship was fitted better by a square law than by a straight line or cubic curve (Fig. 4 E). The same relationship was seen during recovery after M_1R activation (Fig. 4 F, data taken from Jensen et al., 2009). This dependence of KCNQ2/3 current on the square of PH probe FRETr explains why the onset of VSP action on current is faster than that on FRETr. If the decay of FRETr followed an exponential time course with time constant τ, the square of this function would decay exponentially with a time constant of $\tau/2$. It also explains why recovery of current is S shaped and slower than FRETr when fitted with a single exponential (Fig. 4 D). If FRETr recovery followed $y = 1 - \exp(-t/\tau)$, current recovery would follow $y^2 = 1 - 2\exp(-t/\tau) + \exp(-2t/\tau)$, which is S shaped. As predicted by that equation, our recovery data fitted with the double-exponential equation gave mean time constants of 3.1 s for the positive term and 6.8 s for the negative term (Fig. 4 C, inset; 30 cells). This relationship allows us to predict the dependence of KCNQ2/3 current on PIP_2 density from the known PIP_2 affinity of PH probes (Fig. 4 G; for details see Fig. S3), and suggests that more than one PIP_2 molecule binds to activate a KCNQ2/3 channel.

Interestingly, in a few cases (7/31 cells) KCNQ2/3 current recovered after VSP activation to values ~10% higher than the steady-state value before VSP activation. Such over-recovery was observed both with holding at −20 mV and with tail currents. We have so far not investigated what underlies this phenomenon.

Recovery after VSP activation reflects PIP 5-kinase activity

The observations so far might be interpreted in two ways. The straightforward model would be that while VSP is converting PIP_2 into PIP, the depletion of PIP_2 turns off the KCNQ2/3 channels, with a corollary that

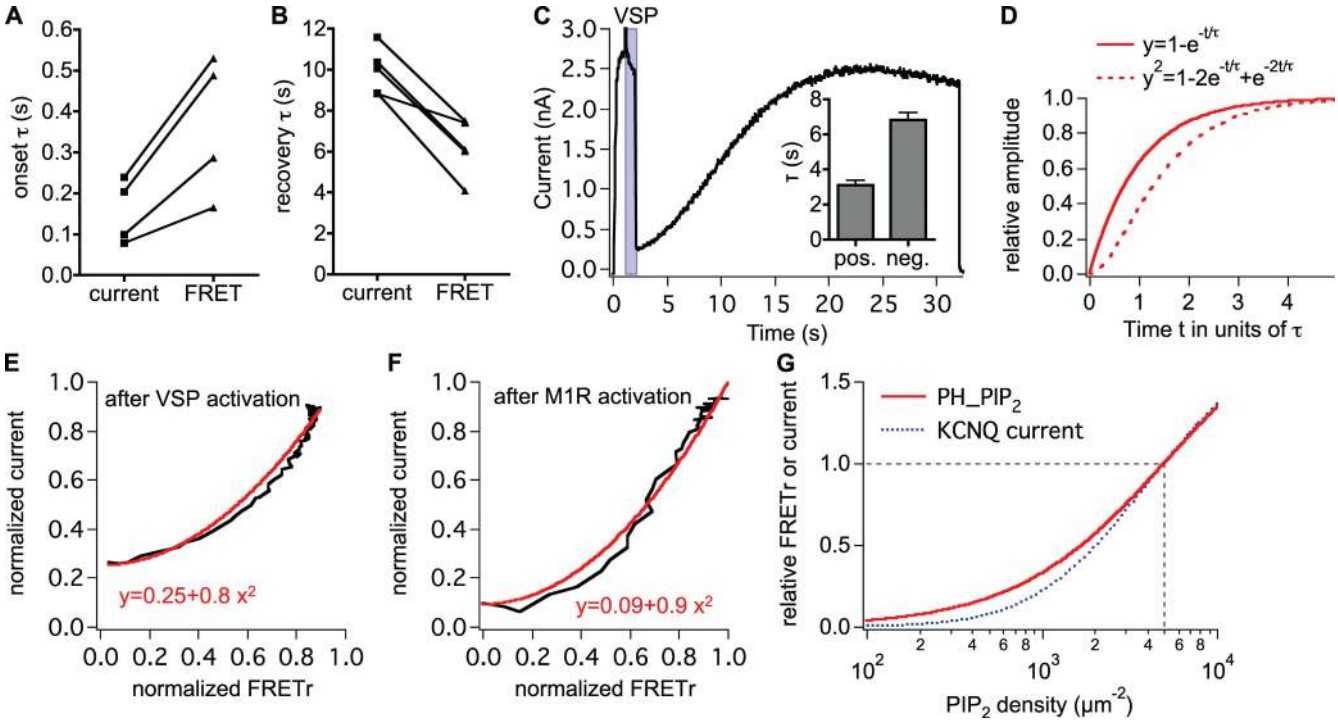

Figure 4. KCNQ2/3 current behaves like the square of PH probe FRET. (A) In four cells, single exponentials were fitted to simultaneously acquired KCNQ2/3 current and PH probe FRETr during VSP activation (2 s of +100 mV). Measurements from the same cell are connected by a line. (B) In five cells, single exponentials were fitted to simultaneously acquired KCNQ2/3 current and PH probe FRETr during recovery after VSP activation. KCNQ2/3 current was measured as tail current amplitude. (C) VSP effect on KCNQ current with voltage protocol as in Fig. 3 B. Recovery of KCNQ2/3 current at −20 mV was fitted with a double exponential: y = a − b*exp(−c*t) + d*exp(−f*t). (Inset) Summary of time constants from 31 cells. Time constant of the positive term (pos.) is 1/f, and that of the negative term (neg.) is 1/c. (D) Illustration of the consequence of squaring an exponential of the form y = 1 − exp(−t/τ). (E) Plot of KCNQ2/3 current at −20 mV (black) versus PH probe FRETr at the same time during recovery after VSP activation in the cell depicted in Fig. 2. Similar observations were made for three other cells. Red curve corresponds to the equation given. (F) Averaged KCNQ2/3 current at −20 mV versus averaged FRETr at the same time after M_1R activation, measured in separate cells (data from Figs. 5 D and 7 B in Jensen et al., 2009). (G) Illustration of the dependence of FRETr (approximated by PH_PIP_2; see Fig. S3) and KCNQ current on PIP_2 concentration as predicted by the model outlined in Fig. 7 and Tables I and II: K_d of PH probe is 2,000 μm^{-2} for PIP_2 and 0.1 μM for IP_3 (0.16 μM IP_3); K_d of KCNQ is 2,000 μm^{-2} for PIP_2. KCNQ current = $(KCNQ\_PIP_2)^2$.

PI(4)P is unable to support activity of the channels. An alternative model would be that channels are directly inhibited by the accumulating pool of PI(4)P rather than by depletion of PIP_2. These possibilities might be distinguished by overexpressing an exogenous PIP 5-kinase to increase tonic PIP_2 levels. In the first model, the increased PIP_2 would make it harder for VSP to deplete PIP_2 quickly and to turn off channels. In the second model, increased PIP_2 might even result in intensified channel inhibition by providing a larger precursor pool for production of inhibitory PI(4)P. As predicted in the first model, we found that the transfected 5-kinase made activation of VSP much less effective at suppressing KCNQ2/3 current (Fig. 5). The relation between the duration of VSP activation and current inhibition was slowed eightfold (Fig. 5, A and B), whereas recovery after VSP activation was speeded fivefold (Fig. 5, A and C). PH probes were not expressed in these experiments. These findings support the concepts that PIP_2 is essential, PI(4)P does not inhibit or permit channel activity, and PI(4)P and the activity of cellular PIP 5-kinase(s) are needed after VSP activation to restore PIP_2 and full channel activity.

Phosphorylation of PI(4)P by PIP 5-kinase is faster than PI(4)P supply by PI 4-kinase

In contrast to VSP, PLC degrades PIP_2 to DAG and IP_3 and also leads to quick PI(4)P depletion (Willars et al., 1998; Horowitz et al., 2005). Recovery after PLC activation needs two steps for PIP_2 resynthesis: first, phosphorylation of PI by a PI 4-kinase, and then phosphorylation of PI(4)P by a PIP 5-kinase. We find that recovery of KCNQ2/3 current after VSP activation (Fig. 6 A) is 5–10-fold faster than recovery after M_1R activation (Fig. 6 E), even when the extent of KCNQ2/3 current inhibition was similar (Fig. 6, C and G). Mean recovery time constants for current were 11 s after VSP activation and 130 s after M_1R activation (Fig. 6, D and H). PH probes were not expressed in either case. The slower recovery after receptor activation cannot be attributed to slow turn

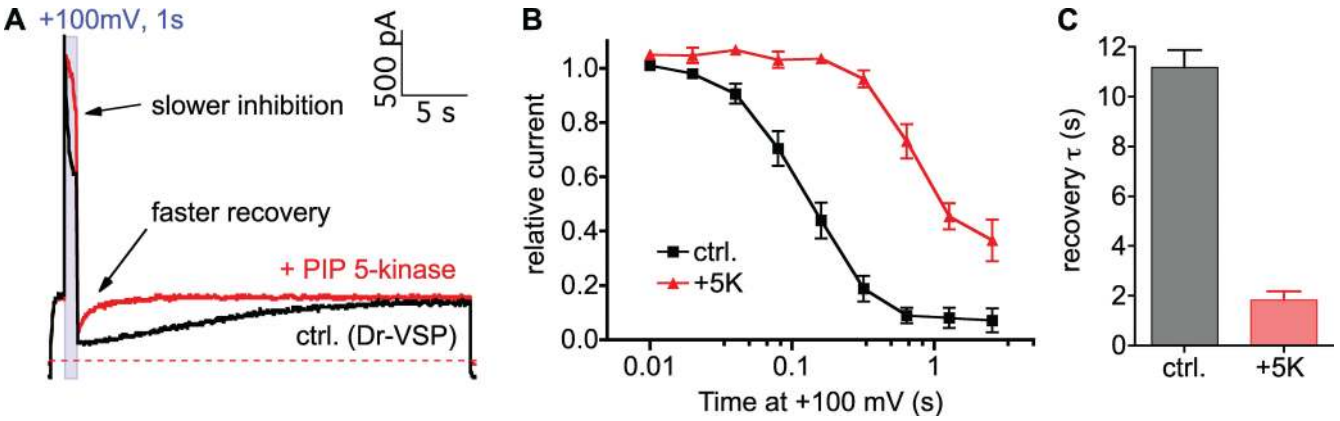

Figure 5. PIP 5-kinase overexpression antagonizes VSP effects. (A) Traces from two cells with similar current amplitudes transfected with Dr-VSP and KCNQ2/3 (ctrl., black trace) or with Dr-VSP, KCNQ2/3, and PIP 5-kinase Iγ (+5K, red trace). (B) Dependence of current inhibition on the duration of VSP activation. Baseline-normalized currents at −20 mV immediately after VSP activation are plotted for control (from Fig. 3 D) and +5K (three cells). (C) Time constants of single-exponential fits to current recovery after VSP activation. Summary of 16 cells for control and 4 cells for +5K.

off of PLC after agonist wash off because the measured interaction of G_q with PLC falls by 95% in only 2 s (Jensen et al., 2009; Falkenburger et al., 2010). Apparently, the production of PI(4)P by PI 4-kinase is rate limiting for recovery after M_1R stimulation, and the endogenous PIP 5-kinase is many-fold faster than the PI 4-kinase.

Modeling of phosphoinositide metabolism, VSP, and PLC

We now return to a quantitative description of the signaling kinetics. For our model of phosphoinositide metabolism (Fig. 7, Tables I and II, and Table S1), we assumed that all phosphoinositide reactions take place in one compartment, and that the relevant kinases and phosphatases obey nonsaturating linear kinetics. For

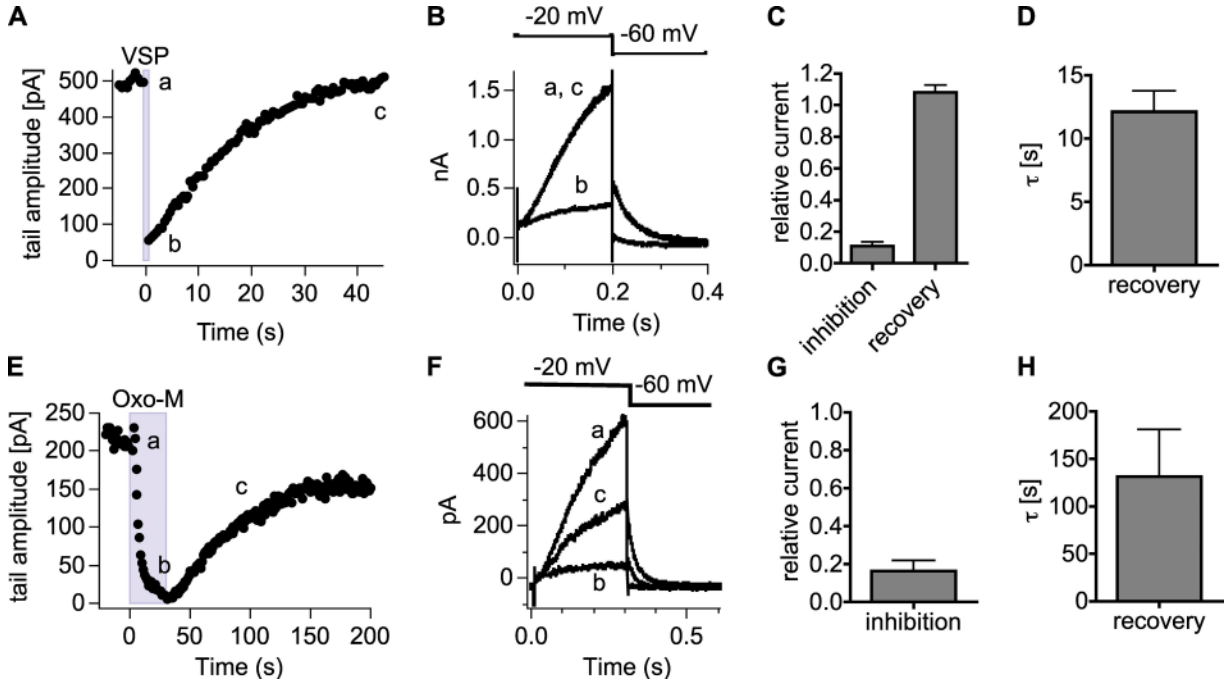

Figure 6. PIP 5-kinase is faster than PI 4-kinase. Tail current amplitudes were used to measure current inhibition by Dr-VSP or M_1R activation and its recovery. (A) Time course of tail current amplitude in a cell transfected with Dr-VSP and KCNQ2/3 (2 points s^{-1}). (B) Superimposed currents at time points before VSP activation (a), after VSP activation (b), and during recovery (c). (C) Summary of tail current amplitudes relative to baseline after VSP activation (b/a) and after recovery (c/a). (D) Time constant of a single-exponential fit to the recovery time course (time b to c). (C and D) Summaries of 19 cells. (E) Time course of tail current amplitudes in a cell transfected with M_1R and KCNQ2/3 (1 point s^{-1}). (F) Superimposed currents at time points a, b, and c indicated in E. (G) Tail current inhibition by M_1R activation (summary of 10 cells). (H) Time constant of an exponential fit of recovery (summary of seven cells).

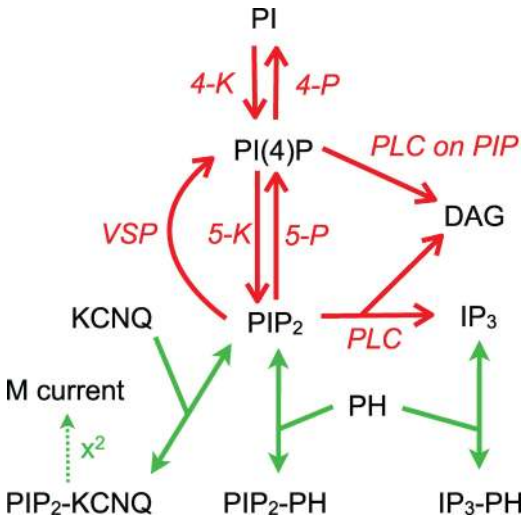

Figure 7. Schematic of the kinetic model. Model species are denoted by Roman letters, and reactions are in italics. Initial conditions and rate constants are listed in Tables I and II, and differential equations are in Table S1. For PIP_2 and IP_3 binding to KCNQ and PH, the association reactions are referred to as forward reactions, and dissociation reactions are referred to as reverse reactions. KCNQ2/3 current depends on the square of PIP_2-bound KCNQ2/3 subunits (PIP_2_KCNQ2/3).

phosphoinositide kinases and phosphatases, we do not know the number of enzyme molecules and so assign a bulk activity rather than a molecular-specific activity. For regulation of KCNQ2/3 current by PIP_2, we implemented a square law as suggested by Fig. 4: KCNQ2/3 subunits bind PIP_2 with the same dissociation constant K_d as PH probes, and KCNQ2/3 current is proportional to the square of the number of PIP_2-bound channel subunits (Fig. 4 G). This implementation closely resembles our earlier model (Suh et al., 2004), where we had a K_d for PIP_2 binding of 1,000 PIP_2 per μm^2 (instead of 2,000) and an exponent of 1.8 (instead of 2). Activation of PLC by M_1Rs was determined by the model described in our companion paper (Falkenburger et al., 2010), which among other things reproduces time course and Oxo-M concentration–response curves for the interaction of $G\alpha_q$ with PLC as measured by FRET (Jensen et al., 2009). As before, our model does not include the well-known contribution of Ca^{2+} as a necessary cofactor in PLC stimulation by G_q (Horowitz et al., 2005).

We began with VSP. It was simple to pick a rate constant for VSP activity that reproduced the rapid time course of KCNQ current inhibition during VSP activation (Fig. 8 A). Then, it was straightforward to set the rate of the endogenous PIP 5-kinase to reproduce current recovery from VSP, which takes ~11 s (Fig. 8 B). This gave us two rate constants and good agreement with the VSP experiments. Fig. 8 C illustrates the decline in PIP_2 and parallel rise in PI(4)P during VSP activation and their recovery hereafter. The choice of PIP 5-kinase rate constant did depend on the uncertain size of the resting PI(4)P pool relative to the PIP_2 pool. If the resting PI(4)P pool was relatively small, the PIP 5-kinase rate constant would have to be a little faster than if the pool was of comparable size to PIP_2 (see Discussion). The new experiments (Fig. 3) also showed that the interaction of PIP_2 with KCNQ channels must be more rapid than we assumed previously.

We then considered strong activation of PLC by M_1R activation. Again, we could easily pick a rate constant for PLC acting on PIP_2 to match the rate of current inhibition by 10 µM Oxo-M (Fig. 9 A, red solid line). Given a target pool size for PI(4)P and the rate constant for the PIP 5-kinase, we could also pick a rate constant for the PI 4-kinase to match the slow recovery from Oxo-M (Fig. 9 B, red solid line). This gave us two more rate constants and a reasonable fit.

Next, we turned to weaker activation of PLC by M_1R activation with subsaturating agonist concentrations.

TABLE I

Initial conditions

Species	Amount	Rationale
R	500 μm^{-2}	From fluorescence[a]
G	40 μm^{-2}	To fit concentration–response curve of current[a]
PLC	10 μm^{-2}	To fit concentration–response curve of current[a]
PI	140,000 μm^{-2}[b]	Xu et al. (2003); Suh et al. (2004)
PIP	4,000 μm^{-2}	Suh et al. (2004); ratio to PIP_2 as in Willars et al. (1998); Winks et al. (2005)
PIP_2	5,000 μm^{-2}	To have 50% PH probes at the membrane, as in Horowitz et al. (2005), similar to Xu et al. (2003)
PH domains[c] (membrane)	3,000 μm^{-2}	From fluorescence[a], similar to Xu et al. (2003)
PH domains[c] (cytosol)	3 µM	1 µM free, 2 µM PH_IP_3; see Fig. S3, similar to Xu et al. (2003)
KCNQ2/3 channels	4 μm^{-2}	From whole cell current, open probability, and single-channel conductance; consistent with Zaika et al. (2008)
IP_3	0.16 µM	Fink et al. (1999); Xu et al. (2003); Winks et al. (2005)

[a]See Falkenburger et al. (2010).
[b]Amount of PI is clamped at 140,000 μm^{-2}.
[c]Not present in all experiments.

TABLE II

Rate constants for phosphoinositide metabolism

Parameter	Value	Units	Rationale
k_PLC	0.1	$\mu m^2\ s^{-1}$	Oxo-M onset of current inhibition
k_PLConPIP	0.14 * k_PLC	$\mu m^2\ s^{-1}$	See Horowitz et al. (2005)
k_PLCbasal	0.0025	s^{-1}	To keep resting IP_3 at 0.16 µM
k_4K	2.6×10^{-4}	s^{-1}	Current recovery after Oxo-M
k_4P	0.006	s^{-1}	To keep PI(4)P levels stable at rest
k_5K	0.02	s^{-1}	Current recovery after VSP
k_5P	0.014	s^{-1}	To keep PIP_2 levels stable at rest
k_VSP[a]	11.3 * f(V)	s^{-1}	Fit to VSP onset, see Fig. S1
speed _KCNQ_PIP_2	0.05	$\mu m^2\ s^{-1}$	Rate limiting if <0.05
KD_KCNQ_PIP_2	2,000	μm^{-2}	As for PH probes
I_KCNQ[b]	a * $(PIP_2\_KCNQ)^2$	pA	See Fig. 4
speed_PH_PIP_2	1	$\mu M^{-1}\ s^{-1}$	Affects timing if <1
KD_PH_PIP_2	2	µM	Lemmon et al. (1995); Hirose et al. (1999); as in Xu et al. (2003); Winks et al. (2005)
speed_PH_IP_3	10	$\mu M^{-1}\ s^{-1}$	To not be rate limiting, from Xu et al. (2003)
KD_PH_IP_3	0.1	µM	Hirose et al. (1999); Lemmon et al. (1995), as in Winks et al. (2005); Xu et al. (2003)
k_IP_3ase	0.08	s^{-1}	From Xu et al. (2003)

Forward reactions of PIP_2 binding are speed_, and reverse reactions are speed_ * KD_; see Table S1.

[a]$f(V) = 1/(1+\exp((-1.5*q_e/k_BT*(V-0.1))))$ with $q_e/k_BT = 25$ mV.

[b]a = channel number * open probability * single-channel current.

This revealed difficulties. Consider the concentration–response relations for Oxo-M inhibition of KCNQ current (data points in Fig. 9 C). The model for G protein activation by receptors and for G protein interaction with PLC is already known to give appropriate concentration–response relations for the early signaling steps (Falkenburger et al., 2010). Hence, it was unexpected that the model did very poorly with the low-concentration responses of the later signaling steps. For KCNQ current, it predicted too much suppression at low Oxo-M concentrations (0.001–1 µM; Fig. 9 C, red solid line). We discuss possible reasons for this discrepancy in the Discussion and show one possible solution here as the green dashed line in Fig. 9 (A–C). In this simulation, the synthesis of new PIP_2 is accelerated several-fold during the Oxo-M application as several authors have already suggested (see Discussion and legend to Fig. 9). Accelerated synthesis counters the PIP_2 depletion catalyzed by weak activation of PLC.

Finally, we considered the actions of Oxo-M on FRET from PH domain probes. The unchanged model (red solid lines) simulates the decrease of FRETr with 10 µM Oxo-M well (Fig. 9 D), and the concentration–response curve moderately well (Fig. 9 F), but it predicts much slower FRETr recovery than is actually seen (Fig. 9 E). Note that these calculations include the effects of 6,000 μm^{-2}

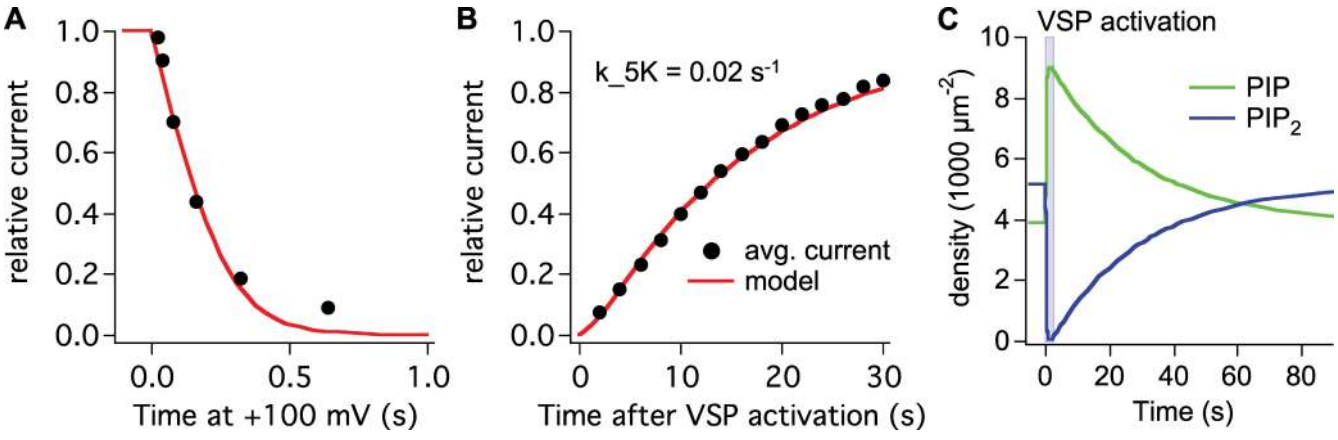

Figure 8. Modeling related to PIP 5-kinase and VSP. Traces are model predictions, and symbols are data. (A) Model current during VSP activation superimposed with the time course of current inhibition from Fig. 3 D. (B) Model current recovery superimposed with averaged time courses as in Fig. 6 A ($n = 11$ cells). (C) Model predictions for PI(4)P and PIP_2 during VSP activation and recovery.

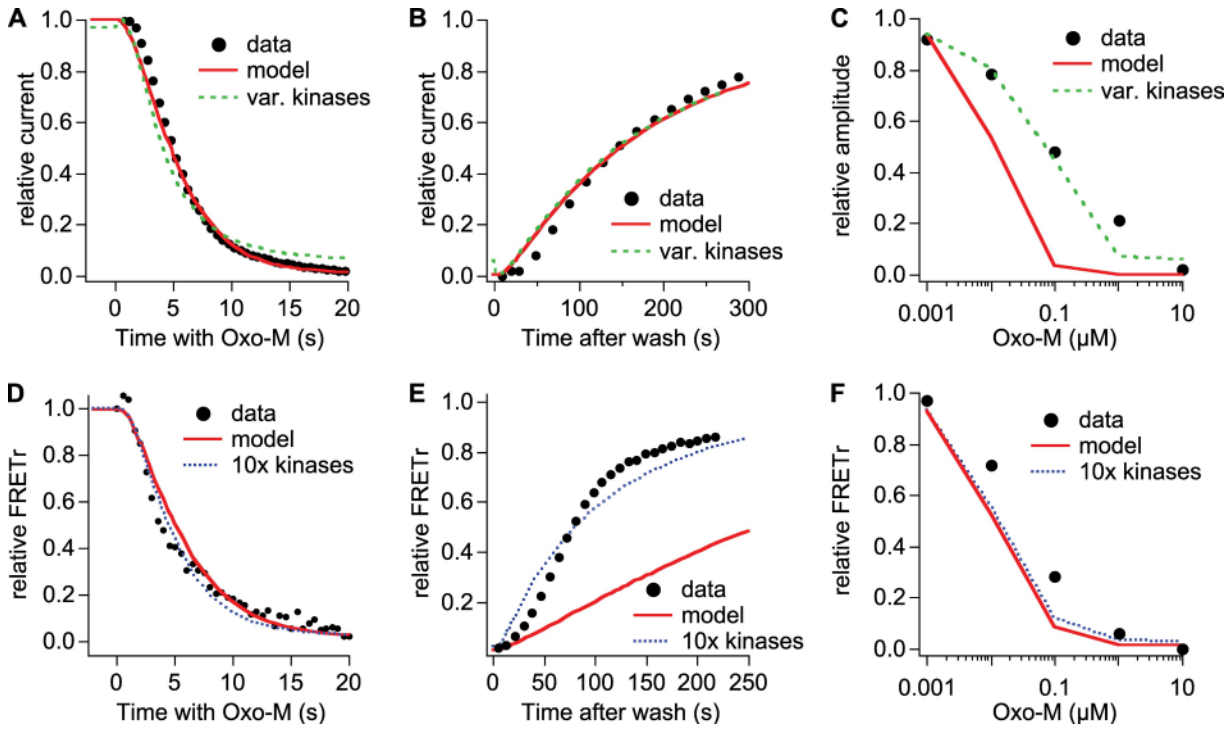

Figure 9. Modeling of PIP_2 depletion by M_1R activation. Symbols are data from Jensen et al. (2009), and lines are model predictions. (A–C) KCNQ2/3 current. (D–F) PH probe FRET. (A and D) Time course of current/FRET inhibition by 10 μM Oxo-M. (B and E) Time course of recovery after M_1R activation. (C and F) Concentration–response curves. Parameters for the red, solid curves are as listed in Tables I and II. For the blue, dotted curves, PI kinases and phosphatases were sped up by 10-fold (k_4K, 2.6×10^{-3} s^{-1}; k_4P, 0.08 s^{-1}; k_5K, 0.2 s^{-1}; k_5P, 0.14 s^{-1}). For the green, dashed curves, the PI 4-kinase was sped up during Oxo-M (but not during recovery) in a manner depending on Oxo-M concentration (2.6×10^{-4} s^{-1} for 0.001 μM, 5×10^{-4} s^{-1} for 0.01 μM, and 2.6×10^{-3} s^{-1} for 0.1 μM and above). k_5K was 0.2 s^{-1} during Oxo-M and 0.02 s^{-1} during recovery. k_4P and k_5P were not accelerated. k_PLC was 0.2 μm^2 s^{-1} to fit onset. PLConPIP was 0.

of PH domains (Falkenburger et al., 2010) that are buffering the PIP_2 as fast as it is made. It is our working hypothesis that in these cells that have been overexpressing PH domain probes as PIP_2 buffers for 2 d, the activity of phosphoinositide-metabolizing enzymes has become augmented by compensatory gene expression. The blue dotted lines show much improvement in fitting the data from assuming that the 4- and 5-kinases and -phosphatases of these cells are augmented 10-fold. Such elevated rates are not appropriate for cells without PH domain expression and, for example, would predict recovery of current after Oxo-M in <20 s.

DISCUSSION

We have completed a kinetic model of M_1R signaling, spanning from the binding of agonist to receptor through G proteins and PLC to PIP_2 depletion and resynthesis. The steps involving receptor and G proteins are described in our companion paper (Falkenburger et al., 2010), and this work adds phosphoinositide metabolism and the gating of KCNQ2/3 current by PIP_2, with aspects of kinase regulation still unresolved. Our experiments lead to several model-independent conclusions. Principal among them are: (1) PIP_2 interaction with KCNQ channels occurs in the millisecond timescale, (2) more than one bound PIP_2 is needed for optimal activation of KCNQ channels, and (3) PIP_2 recovery after VSP activation is much faster than after PLC activation.

Gating of KCNQ2/3 current by PIP_2

Activation of Dr-VSP reduces PIP_2 rapidly. KCNQ2/3 current responds to VSP activations as short as 40 ms, even before the sensing charge movement has finished. The rapidity of the inhibition means that PIP_2 exchange at KCNQ2/3 channels is fast. In our earlier models (e.g., Suh et al., 2004), the residence time of PIP_2 on a channel subunit was set at 4 s, but we had little evidence to go on. The VSP result here shows that 4 s is much too long because channel inhibition reaches a new steady level within tens of milliseconds after each VSP activation (Fig. 3 C). In the revised model, the residence time of PIP_2 is 10 ms. It could be made shorter but not much longer. Apparently, the turnover time of PIP_2 lipids on KCNQ subunits is shorter than the macroscopic gating times of the channel and is more on a timescale appropriate to underlie open–close transitions at the single-channel level, as was assumed by Park et al. (2005). This conclusion is predicated on the assumption that PIP_2

must dissociate from channel subunits before VSP can cleave the 5-phosphate. Given that the PIP_2 binding site at VSP is buried in the enzyme molecule (Okamura et al., 2009), this assumption appears reasonable.

Recovery of PIP_2 and current after VSP activation was slow enough (10–20 s) to assume that KCNQ2/3 channels remain near equilibrium with PIP_2 throughout as the PIP_2 is restored gradually. The nonlinear relationship of KCNQ2/3 current to PH probe FRETr indicates that current behaves like the square of the PH probe FRETr and explains why KCNQ2/3 current turns off faster than PH probe FRETr during PIP_2 depletion. Such an accelerated turn-off might be biologically relevant as a way to speed the loss of KCNQ2/3 current and the increase of neuronal excitability in response to receptor activation. The cooperativity in PIP_2 activation of KCNQ2/3 channels seen here in intact cells is consistent with Hill coefficients in the range of 1.35 to 1.9 for current activation obtained by application of (short-chain) diC_8-PIP_2 to excised inside-out membrane patches (Zhang et al., 2003; Li et al., 2005).

Very few KCNQ2/3 channels are needed to measure PIP_2—only around four channels μm^{-2} in our cells, based on whole cell current, open probability, and single-channel conductance (see also Zaika et al. 2008). That small number would not perturb the cellular PIP_2 pools; however, Zaika et al. (2008) report that for every electrophysiologically functional KCNQ channel, there can be many additional channels in the plasma membrane that do not contribute to current. Quite likely they would also bind PIP_2. In contrast, PH probes require a high density to work as FRET reporters (Fig. S3 B): 1,700–3,000 μm^{-2} for each PH probe (PH-CFP and PH-YFP) as determined by FRET efficiency and fluorescence intensity (Falkenburger et al., 2010). The pool of PIP_2 bound to the two PH probes is thus significant as compared with the pool of free PIP_2, which we take to be 5,000 μm^{-2}. This can alter phosphoinositide dynamics, as we and others find (Holz et al., 2000; Raucher et al., 2000; Lei et al., 2001; Várnai et al., 2002; Gamper et al., 2004; Szentpetery et al., 2009). The inhibition of KCNQ2/3 current by M_1R activation was slower, and the recovery faster, in cells with PH probe expression (Fig. 7 in Jensen et al., 2009). The slower onset of current inhibition with PH probe expression is reproduced by the model (not depicted). It is explained by buffering of PIP_2 by PH probes providing a reserve of PIP_2 to be hydrolyzed; however, our model does not predict a faster recovery of KCNQ2/3 current with PH probe expression unless the rates of some steps are modified. It also does not reproduce a relatively fast recovery of PH probe FRETr seen after M_1R activation (Jensen et al., 2009). Such deviations from our simple predictions suggest that chronic expression of PH probes induces compensatory changes in phosphoinositide metabolism (see below).

Phosphoinositide pools

Full interpretation of phosphoinositide kinetics is limited by uncertainty about the absolute endogenous levels of different phosphoinositide lipids and the enzymes that act on them at the plasma membrane and in other membranes. We begin with the lipids.

Even for PIP_2, the density at the plasma membrane remains uncertain. McLaughlin et al. (2002) and Golebiewska et al. (2008) suggest an effective free concentration of 10 µM referred to total cell volume, which is equivalent to ~10,000 μm^{-2} at the membrane for the 10-µm diameter cell they had in mind. Xu et al. (2003) give 4,000 μm^{-2}, and Hilgemann (2007) suggests values of 20,000–60,000 μm^{-2}. These estimates include potential errors in determining the total lipid content of a sample, the count of cells in the sample, and the plasma membrane area of each cell. According to measurements of PIP_2 diffusion by fluorescence correlation spectroscopy (Golebiewska et al., 2008), only one third of all PIP_2 (the 10 µM above) is free, and two thirds is reversibly bound to membrane proteins with an exchange time of ~10 ms. In all our calculations, we assume that reactions of probes and enzymes like PIP_2 5-phosphatase and PLC are restricted to free PIP_2 molecules. Here and before (Suh et al., 2004), we have assumed 5,000 free PIP_2 μm^{-2} in our modeling. This number would be compatible with the observation that ~50% of PH domains are bound to the plasma membrane and 50% are in the cytosol (Stauffer et al., 1998; van der Wal et al., 2001; Xu et al., 2003; Horowitz et al., 2005; Winks et al., 2005), with the following two assumptions: the in vitro dissociation constants for the binding of PIP_2 and of IP_3 to PH domains are valid, and the resting IP_3 concentration in the cell is 0.16 µM (Fink et al., 1999; Xu et al., 2003; Winks et al., 2005; see Fig. S3 A). Had we assumed a high PIP_2 density (20,000–60,000 μm^{-2}), the expression of a pair of PH probes at 1,700–3,000 μm^{-2} each would have had little impact on PIP_2 dynamics, so we consider this discrepancy as an argument against such high densities.

Biochemical measurements of PI and PI(4)P are even more difficult to interpret. Where are the pools of these PIP_2 precursors, how big are they, and where are the enzymes that act on them? The total cellular content of PI(4)P is similar to that of PIP_2 (Willars et al., 1998; Nasuhoglu et al., 2002; Horowitz et al., 2005). We have suggested before that the pool of PI(4)P that is accessible to PLC during a 60-s M_1R activation (88% of the total) might all be at the plasma membrane (Horowitz et al., 2005). However, lipid trafficking from cytosolic vesicles to the plasma membrane might be fast enough ($t_{1/2}$ = 2 min; Maxfield and McGraw, 2004) to confound this concept. Some studies support the assumption that the majority of PI(4)P is at the plasma membrane (Hammond et al., 2009), but this could contradict the notion that PI(4)P is the characteristic phosphoinositide

of the Golgi complex and secretory vesicles. Endogenous PI 4-kinase activity is primarily associated with Golgi membranes, and overexpressed, fluorescently tagged type III PI 4-kinases localize primarily to ER and Golgi, but not to the plasma membrane (Cockcroft et al., 1985; Zhao et al., 2001; Wenk and De Camilli, 2004; Balla, 2007). Further, phosphoinositide transport proteins have been found necessary for sustained IP_3 generation in HL60 cells (Cunningham et al., 1995). These findings suggest that levels of PI(4)P at the plasma membrane might be low (<<88% of total PI(4)P), and that transfer of PI(4)P between membrane compartments might be rapid. However, no phosphoinositide transport proteins have been reported for PI(4)P so far. (Phosphoinositide transport proteins might also act as cofactors for lipid kinases at the plasma membrane; Wirtz, 1997.)

Our kinetic model contains a single pool of PI(4)P in the same kinetic compartment as PIP_2. We have determined relative reaction fluxes from our time courses but have to remain skeptical about the absolute rate constants and absolute fluxes as long as the size and distribution of the PI(4)P pool(s) are unknown. Perhaps it is more realistic to represent the PI(4)P pool as several compartments connected by transport steps and to reinterpret the "synthesis" of PI(4)P by step *4-K* in the model as including influx of PI(4)P from other compartments.

Metabolism of phosphoinositides

Ci-VSP has been shown to act as a PIP 5-phosphatase, both by biochemical assays and by monitoring PIP_2 and PI(4)P with fluorescent probes (Iwasaki et al., 2008; Halaszovich et al., 2009), implying that Dr-VSP also would act as a PIP 5-phosphatase. This is consistent with our observations that overexpression of PIP 5-kinase makes VSP activation less effective in suppressing current, requiring stronger depolarization to produce the same effect, and that recovery after VSP activation is speeded by overexpression of the PIP 5-kinase. VSP-sensing currents suggest that 13,000 VSP molecules are expressed per μm^2 of membrane, 50% of which are activated at +100 mV. As the number of activated VSP molecules (6,500 μm^{-2}) may surpass that of PIP_2 molecules, VSP might "deplete" all PIP_2 simply by binding them before completing a full cycle of enzymatic activity. Thus, the rapid burst of current inhibition by VSP might overestimate the maximum velocity of steady-state VSP action. In our model, the initial PIP_2 consumption rate for VSP (at +100 mV) is 28,000 $s^{-1}\mu m^{-2}$. For comparison, the cleavage rate with endogenous PLC during M_1R activation is 35-fold slower in the model, around 800 $s^{-1}\mu m^{-2}$. The few PLC molecules (10 μm^{-2}) would have to undergo many turnover cycles to deplete PIP_2 over the course of a few seconds.

Because VSP is a 5-phosphatase, recovery of PIP_2 and KCNQ current is governed by cellular PIP 5-kinases. All of the depolarization-induced 5-phosphatase activity has to be from the plasma membrane VSP that the patch clamp voltage controls. Therefore, at least the PI(4)P generated by VSP activity and the PIP 5-kinase needed for rapid (few seconds) rephosphorylation should be in the plasma membrane. The chosen 5-kinase rate constant (0.02 s^{-1}), which depends on our assumption of initial plasma membrane PI(4)P, is in a similar range as in previous models (0.045 s^{-1} in Horowitz et al., 2005; 0.048 s^{-1} in Xu et al., 2003).

The 5-kinase could be regulated. M_1R activation can activate Rho kinase (Dutt et al., 2002), and several studies have shown stimulation of PIP 5-kinases by Rho family kinases and other signaling events (for review see Oude Weernink et al., 2004; Santarius et al., 2006; Mao and Yin, 2007). Measuring lipid and IP_3 turnover in response to muscarinic agonists, Willars et al. (1998) found: (1) both PIP_2 and PI(4)P are depleted quickly (as we also found; Horowitz et al., 2005), (2) yet IP_3 continues to be made in long stimulations, and (3), surprisingly, PIP_2 recovers before PIP. The more rapid recovery of PIP_2 might be explained by strong transient stimulation of PIP 5-kinase (and not the 5-phosphatase) during the recovery period. The extensive depletion of PI(4)P during receptor activation has at least two possible explanations. Accelerated 5-kinase could be converting the PI(4)P pool to PIP_2 that is then cleaved by PLC, or PLC might accept PI(4)P as a substrate in addition to PIP_2 (Wilson et al., 1984). Here, as before (Horowitz et al., 2005), our model assumes that PLC is able to cleave PI(4)P slowly (Table II), but we also suggest that speeding the 5-kinase during receptor activation helps explain the concentration–response relation for current (Fig. 9 C). Nevertheless, our measurements and modeling do not provide a clear preference for assuming that PLC does or does not cleave PI(4)P significantly. Removing the assumption forced changes in other rate constants but did not improve the fitting of, for example, the concentration–response curves.

Recovery after M_1R activation requires a wortmannin-sensitive (type III) PI 4-kinase (Suh and Hille, 2002; Zhang et al., 2003; Winks et al., 2005); therefore, we called the step that supplies PI(4)P at the membrane "*4-K*." This step may also be accelerated by receptor activation. Stimulation of PI 4-kinase by receptor activation has been invoked in studies estimating IP_3 production (e.g., Cunningham et al., 1995; Willars et al., 1998; Xu et al., 2003; Brown et al., 2008) and by the failure of bradykinin and purinergic agonists to deplete PIP_2 despite activating PLC in neurons (Gamper et al., 2004; Zaika et al., 2007). We also suggest a faster rate for this step during Oxo-M than during recovery to reproduce our data with subsaturating Oxo-M (Fig. 9, A–C, green dashed lines; see also details in the legend). It would prevent low agonist concentrations from depleting PIP_2 excessively. If PI 4-kinase and PIP 5-kinase are stimulated

by receptor activation, we do not know how long that effect lasts after agonist is removed. Hence, our estimates of their rates after agonist removal may be imperfect. (We expect no acceleration of kinases by VSP activation.) Current recovery from agonist was faster after overexpression of PLC or PH probes (Jensen et al., 2009). In these cases, however, the speeding might represent compensatory gene expression.

What is the mechanism of receptor-induced stimulation of PI(4)P synthesis? The speeding of PI 4-kinase by bradykinin requires IP_3-mediated calcium release and neuronal calcium sensor 1 (Gamper et al., 2004; Zaika et al., 2007). Calmodulin-like neuronal calcium sensor 1 binds to PI 4-kinase β (in the Golgi) and stimulates the 4-kinase activity when calcium is increased by receptor activation (Zhao et al., 2001; Koizumi et al., 2002; Pan et al., 2002; Winks et al., 2005). The stimulation can be so strong that PIP_2 is not depleted despite PLC activation. It is possible that M_1R activation, which makes a Ca^{2+} transient in tsA201 cells, stimulates PI 4-kinase by a similar mechanism, but to a lesser extent. There might also be other messengers. If type III PI 4-kinases are located in the Golgi complex, it is possible that not the PI 4-kinase but the PI(4)P transport to the plasma membrane might be rate limiting and stimulated by receptor activation. Our model would not discriminate between the stimulation of PI 4-kinases and any other event that transiently increases plasma membrane PI(4)P. One such possibility is exocytosis. Secretory vesicles are thought to bear PI(4)P formed by PI 4-kinases in Golgi and by 5-phosphatases during endocytosis (De Matteis and Godi, 2004; Wenk and De Camilli, 2004; Balla et al., 2005). Exocytosis can increase upon stimulation of $G\alpha_q$-coupled receptors both by Ca^{2+} release and by activating PKC (e.g., Hille et al., 1999), and vesicle fusion with the plasma membrane would deliver PI(4)P to the plasma membrane.

The time course of Oxo-M effects on PH probe FRET was well reproduced with increased rates for PIP_2 synthesis (Fig. 9, D–F, dotted traces). Interestingly, the acceleration had little effect on the depression of PH probe FRET by Oxo-M (Fig. 9, D and F, dotted line vs. solid line). The reason is that PH probe FRET also responds to production of a second ligand, IP_3, whereas current depends only on PIP_2.

We proposed receptor-induced acceleration of PIP_2 synthesis in part to correct a discrepancy in the predicted agonist concentration–response curve and in part because it is frequently invoked in the literature. The discrepancy was that low concentrations of agonist suppressed currents too much in the model as if PLC were activated too strongly there. Now we suggest a second factor that is likely to contribute to this discrepancy as well. Strong stimulation of M_1Rs in tsA cells invokes a Ca^{2+} transient (via IP_3) that accelerates PLC strongly in a positive feedback loop (Horowitz et al., 2005). In our model, PLC activity depends on $G\alpha_q$, but the Ca^{2+} dependence is omitted. At low agonist concentrations, the IP_3 and Ca^{2+} positive feedback should be much less, so our model will overestimate the stimulation of PLC there. This defect cannot be modeled until we study how IP_3 production, Ca^{2+} elevation, and feedback to PLC depend on receptor activation. At high agonist concentrations, the time it takes to produce a full Ca^{2+} elevation might also contribute to a small delay we see in the onset of current suppression after agonist application (Table I in Jensen et al., 2009).

Conclusions

We have constructed a kinetic model of phosphoinositide metabolism informed by new kinetic studies after rapid dephosphorylation of PIP_2 by Dr-VSP. Although this model represents a substantial advance from the previous one, it also shows clearly where we have to learn more. We need better estimates of phosphoinositide amounts in different membrane compartments and to determine the extent to which compartments other than the plasma membrane are involved in M_1R signaling and lipid dynamics. In particular, the step supplying PI(4)P at the plasma membrane remains elusive. It is possible that events other than phosphorylation of PI at the plasma membrane contribute to the timing. We have shown that the step synthesizing PIP_2 from PIP is much faster than the preceding step that supplies PIP, and we have advanced understanding of how PIP_2 binding allows KCNQ2/3 channels to open. More than one PIP_2 is needed per channel, and the residence time on a channel subunit is <10 ms. This insight is valuable for using KCNQ2/3 current to monitor cellular PIP_2 levels and might generalize to other PIP_2-regulated ion channels. Finally, we have shown that the voltage regulation of VSP activity is fast and makes VSP a powerful tool for investigating and perturbing phosphoinositide physiology and metabolism.

We thank Yasushi Okamura for providing Ci-VSP and Dr-VSP, Erwin Neher and William Zagotta for commenting on the manuscript, Sharona E. Gordon for use of equipment, and Lea Miller for technical help.

The Virtual Cell is supported by National Institutes of Health (NIH) grant P41RR013186 from the National Center for Research Resources. Our work was supported by NIH grants R01 NS08174, R01 GM83913, and T32 GM07108, and the Human Frontier Science Program.

Edward N. Pugh Jr. served as editor.

Submitted: 14 October 2009
Accepted: 18 December 2009

REFERENCES

Akemann, W., A. Lundby, H. Mutoh, and T. Knöpfel. 2009. Effect of voltage sensitive fluorescent proteins on neuronal excitability. *Biophys. J.* 96:3959–3976. doi:10.1016/j.bpj.2009.02.046

Balla, T. 2007. Imaging and manipulating phosphoinositides in living cells. *J. Physiol.* 582:927–937. doi:10.1113/jphysiol.2007.132795

Balla, A., G. Tuymetova, A. Tsiomenko, P. Várnai, and T. Balla. 2005. A plasma membrane pool of phosphatidylinositol 4-phosphate is generated by phosphatidylinositol 4-kinase type-III alpha: studies with the PH domains of the oxysterol binding protein and FAPP1. *Mol. Biol. Cell.* 16:1282–1295. doi:10.1091/mbc.E04-07-0578

Brown, S.A., F. Morgan, J. Watras, and L.M. Loew. 2008. Analysis of phosphatidylinositol-4,5-bisphosphate signaling in cerebellar Purkinje spines. *Biophys. J.* 95:1795–1812.

Chong, L.D., A. Traynor-Kaplan, G.M. Bokoch, and M.A. Schwartz. 1994. The small GTP-binding protein Rho regulates a phosphatidylinositol 4-phosphate 5-kinase in mammalian cells. *Cell.* 79:507–513. doi:10.1016/0092-8674(94)90259-3

Cockcroft, S., J.A. Taylor, and J.D. Judah. 1985. Subcellular localisation of inositol lipid kinases in rat liver. *Biochim. Biophys. Acta.* 845:163–170. doi:10.1016/0167-4889(85)90173-9

Corry, B., D. Jayatilaka, and P. Rigby. 2005. A flexible approach to the calculation of resonance energy transfer efficiency between multiple donors and acceptors in complex geometries. *Biophys. J.* 89:3822–3836. doi:10.1529/biophysj.105.069351

Cunningham, E., G.M. Thomas, A. Ball, I. Hiles, and S. Cockcroft. 1995. Phosphatidylinositol transfer protein dictates the rate of inositol trisphosphate production by promoting the synthesis of PIP_2. *Curr. Biol.* 5:775–783. doi:10.1016/S0960-9822(95)00154-0

De Matteis, M.A., and A. Godi. 2004. PI-loting membrane traffic. *Nat. Cell Biol.* 6:487–492. doi:10.1038/ncb0604-487

Di Paolo, G., and P. De Camilli. 2006. Phosphoinositides in cell regulation and membrane dynamics. *Nature.* 443:651–657. doi:10.1038/nature05185

Dutt, P., L. Kjoller, M. Giel, A. Hall, and D. Toksoz. 2002. Activated Gαq family members induce Rho GTPase activation and Rho-dependent actin filament assembly. *FEBS Lett.* 531:565–569. doi:10.1016/S0014-5793(02)03625-6

Falkenburger, B.H., J.B. Jensen, and B. Hille. 2010. Kinetics of M_1 muscarinic receptor signaling to phospholipase C in living cells. *J. Gen. Physiol.* 135:81–97.

Fink, C.C., B. Slepchenko, and L.M. Loew. 1999. Determination of time-dependent inositol-1,4,5-trisphosphate concentrations during calcium release in a smooth muscle cell. *Biophys. J.* 77:617–628. doi:10.1016/S0006-3495(99)76918-3

Fung, B.K., and L. Stryer. 1978. Surface density determination in membranes by fluorescence energy transfer. *Biochemistry.* 17:5241–5248. doi:10.1021/bi00617a025

Gamper, N., V. Reznikov, Y. Yamada, J. Yang, and M.S. Shapiro. 2004. Phosphatidylinositol 4,5-bisphosphate signals underlie receptor-specific $G_{q/11}$-mediated modulation of N-type Ca^{2+} channels. *J. Neurosci.* 24:10980–10992. doi:10.1523/JNEUROSCI.3869-04.2004

Golebiewska, U., M. Nyako, W. Woturski, I. Zaitseva, and S. McLaughlin. 2008. Diffusion coefficient of fluorescent phosphatidylinositol 4,5-bisphosphate in the plasma membrane of cells. *Mol. Biol. Cell.* 19:1663–1669. doi:10.1091/mbc.E07-12-1208

Halaszovich, C.R., D.N. Schreiber, and D. Oliver. 2009. Ci-VSP is a depolarization-activated phosphatidylinositol-4,5-bisphosphate and phosphatidylinositol-3,4,5-trisphosphate 5′-phosphatase. *J. Biol. Chem.* 284:2106–2113. doi:10.1074/jbc.M803543200

Hammond, G.R., G. Schiavo, and R.F. Irvine. 2009. Immunocytochemical techniques reveal multiple, distinct cellular pools of PtdIns4P and PtdIns(4,5)P_2. *Biochem. J.* 422:23–35. doi:10.1042/BJ20090428

Hilgemann, D.W. 2007. Local PIP_2 signals: when, where, and how? *Pflugers Arch.* 455:55–67. doi:10.1007/s00424-007-0280-9

Hilgemann, D.W., and R. Ball. 1996. Regulation of cardiac Na^+,Ca^{2+} exchange and K_{ATP} potassium channels by PIP_2. *Science.* 273:956–959. doi:10.1126/science.273.5277.956

Hilgemann, D.W., S. Feng, and C. Nasuhoglu. 2001. The complex and intriguing lives of PIP_2 with ion channels and transporters. *Sci. STKE.* 2001:re19. doi:10.1126/stke.2001.111.re19

Hille, B., J. Billiard, D.F. Babcock, T. Nguyen, and D.S. Koh. 1999. Stimulation of exocytosis without a calcium signal. *J. Physiol.* 520:23–31. doi:10.1111/j.1469-7793.1999.00023.x

Hirose, K., S. Kadowaki, M. Tanabe, H. Takeshima, and M. Iino. 1999. Spatiotemporal dynamics of inositol 1,4,5-trisphosphate that underlies complex Ca^{2+} mobilization patterns. *Science.* 284:1527–1530. doi:10.1126/science.284.5419.1527

Holz, R.W., M.D. Hlubek, S.D. Sorensen, S.K. Fisher, T. Balla, S. Ozaki, G.D. Prestwich, E.L. Stuenkel, and M.A. Bittner. 2000. A pleckstrin homology domain specific for phosphatidylinositol 4, 5-bisphosphate (PtdIns-4,5-P_2) and fused to green fluorescent protein identifies plasma membrane PtdIns-4,5-P_2 as being important in exocytosis. *J. Biol. Chem.* 275:17878–17885. doi:10.1074/jbc.M000925200

Horowitz, L.F., W. Hirdes, B.C. Suh, D.W. Hilgemann, K. Mackie, and B. Hille. 2005. Phospholipase C in living cells: activation, inhibition, Ca^{2+} requirement, and regulation of M current. *J. Gen. Physiol.* 126:243–262. doi:10.1085/jgp.200509309

Hossain, M.I., H. Iwasaki, Y. Okochi, M. Chahine, S. Higashijima, K. Nagayama, and Y. Okamura. 2008. Enzyme domain affects the movement of the voltage sensor in ascidian and zebrafish voltage-sensing phosphatases. *J. Biol. Chem.* 283:18248–18259. doi:10.1074/jbc.M706184200

Iwasaki, H., Y. Murata, Y. Kim, M.I. Hossain, C.A. Worby, J.E. Dixon, T. McCormack, T. Sasaki, and Y. Okamura. 2008. A voltage-sensing phosphatase, Ci-VSP, which shares sequence identity with PTEN, dephosphorylates phosphatidylinositol 4,5-bisphosphate. *Proc. Natl. Acad. Sci. USA.* 105:7970–7975. doi:10.1073/pnas.0803936105

Jensen, J.B., J.S. Lyssand, C. Hague, and B. Hille. 2009. Fluorescence changes reveal kinetic steps of muscarinic receptor–mediated modulation of phosphoinositides and Kv7.2/7.3 K^+ channels. *J. Gen. Physiol.* 133:347–359. doi:10.1085/jgp.200810075

Koizumi, S., P. Rosa, G.B. Willars, R.A. Challiss, E. Taverna, M. Francolini, M.D. Bootman, P. Lipp, K. Inoue, J. Roder, and A. Jeromin. 2002. Mechanisms underlying the neuronal calcium sensor-1-evoked enhancement of exocytosis in PC12 cells. *J. Biol. Chem.* 277:30315–30324. doi:10.1074/jbc.M201132200

Lei, Q., E.M. Talley, and D.A. Bayliss. 2001. Receptor-mediated inhibition of G protein-coupled inwardly rectifying potassium channels involves $G\alpha_q$ family subunits, phospholipase C, and a readily diffusible messenger. *J. Biol. Chem.* 276:16720–16730. doi:10.1074/jbc.M100207200

Lemmon, M.A., K.M. Ferguson, R. O'Brien, P.B. Sigler, and J. Schlessinger. 1995. Specific and high-affinity binding of inositol phosphates to an isolated pleckstrin homology domain. *Proc. Natl. Acad. Sci. USA.* 92:10472–10476. doi:10.1073/pnas.92.23.10472

Li, Y., N. Gamper, D.W. Hilgemann, and M.S. Shapiro. 2005. Regulation of Kv7 (KCNQ) K^+ channel open probability by phosphatidylinositol 4,5-bisphosphate. *J. Neurosci.* 25:9825–9835. doi:10.1523/JNEUROSCI.2597-05.2005

Mao, Y.S., and H.L. Yin. 2007. Regulation of the actin cytoskeleton by phosphatidylinositol 4-phosphate 5 kinases. *Pflugers Arch.* 455:5–18. doi:10.1007/s00424-007-0286-3

Maxfield, F.R., and T.E. McGraw. 2004. Endocytic recycling. *Nat. Rev. Mol. Cell Biol.* 5:121–132. doi:10.1038/nrm1315

McLaughlin, S., J. Wang, A. Gambhir, and D. Murray. 2002. PIP_2 and proteins: interactions, organization, and information flow. *Annu. Rev. Biophys. Biomol. Struct.* 31:151–175. doi:10.1146/annurev.biophys.31.082901.134259

Murata, Y., and Y. Okamura. 2007. Depolarization activates the phosphoinositide phosphatase Ci-VSP, as detected in Xenopus oocytes coexpressing sensors of PIP_2. *J. Physiol.* 583:875–889. doi:10.1113/jphysiol.2007.134775

Murata, Y., H. Iwasaki, M. Sasaki, K. Inaba, and Y. Okamura. 2005. Phosphoinositide phosphatase activity coupled to an intrinsic voltage sensor. *Nature.* 435:1239–1243. doi:10.1038/nature03650

Nakanishi, S., K.J. Catt, and T. Balla. 1995. A wortmannin-sensitive phosphatidylinositol 4-kinase that regulates hormone-sensitive pools of inositolphospholipids. *Proc. Natl. Acad. Sci. USA.* 92:5317–5321. doi:10.1073/pnas.92.12.5317

Nasuhoglu, C., S. Feng, J. Mao, M. Yamamoto, H.L. Yin, S. Earnest, B. Barylko, J.P. Albanesi, and D.W. Hilgemann. 2002. Nonradioactive analysis of phosphatidylinositides and other anionic phospholipids by anion-exchange high-performance liquid chromatography with suppressed conductivity detection. *Anal. Biochem.* 301:243–254. doi:10.1006/abio.2001.5489

Okamura, Y., Y. Murata, and H. Iwasaki. 2009. Voltage-sensing phosphatase: actions and potentials. *J. Physiol.* 587:513–520. doi:10.1113/jphysiol.2008.163097

Oude Weernink, P.A., M. Schmidt, and K.H. Jakobs. 2004. Regulation and cellular roles of phosphoinositide 5-kinases. *Eur. J. Pharmacol.* 500:87–99. doi:10.1016/j.ejphar.2004.07.014

Pan, C.Y., A. Jeromin, K. Lundstrom, S.H. Yoo, J. Roder, and A.P. Fox. 2002. Alterations in exocytosis induced by neuronal Ca^{2+} sensor-1 in bovine chromaffin cells. *J. Neurosci.* 22:2427–2433.

Park, K.-H., J. Piron, S. Dahimene, J. Mérot, I. Baró, D. Escande, and G. Loussouarn. 2005. Impaired KCNQ1-KCNE1 and phosphatidylinositol-4,5-bisphosphate interaction underlies the long QT syndrome. *Circ. Res.* 96:730–739. doi:10.1161/01.RES.0000161451.04649.a8

Patterson, G., R.N. Day, and D. Piston. 2001. Fluorescent protein spectra. *J. Cell Sci.* 114:837–838.

Raucher, D., T. Stauffer, W. Chen, K. Shen, S. Guo, J.D. York, M.P. Sheetz, and T. Meyer. 2000. Phosphatidylinositol 4,5-bisphosphate functions as a second messenger that regulates cytoskeleton-plasma membrane adhesion. *Cell.* 100:221–228. doi:10.1016/S0092-8674(00)81560-3

Santarius, M., C.H. Lee, and R.A. Anderson. 2006. Supervised membrane swimming: small G-protein lifeguards regulate PIPK signalling and monitor intracellular PtdIns(4,5)P_2 pools. *Biochem. J.* 398:1–13. doi:10.1042/BJ20060565

Stauffer, T.P., S. Ahn, and T. Meyer. 1998. Receptor-induced transient reduction in plasma membrane PtdIns(4,5)P_2 concentration monitored in living cells. *Curr. Biol.* 8:343–346. doi:10.1016/S0960-9822(98)70135-6

Suh, B.C., and B. Hille. 2002. Recovery from muscarinic modulation of M current channels requires phosphatidylinositol 4,5-bisphosphate synthesis. *Neuron.* 35:507–520. doi:10.1016/S0896-6273(02)00790-0

Suh, B.C., and B. Hille. 2008. PIP_2 is a necessary cofactor for ion channel function: how and why? *Annu Rev Biophys.* 37:175–195. doi:10.1146/annurev.biophys.37.032807.125859

Suh, B.C., L.F. Horowitz, W. Hirdes, K. Mackie, and B. Hille. 2004. Regulation of KCNQ2/KCNQ3 current by G protein cycling: the kinetics of receptor-mediated signaling by G_q. *J. Gen. Physiol.* 123:663–683. doi:10.1085/jgp.200409029

Szentpetery, Z., A. Balla, Y.J. Kim, M.A. Lemmon, and T. Balla. 2009. Live cell imaging with protein domains capable of recognizing phosphatidylinositol 4,5-bisphosphate; a comparative study. *BMC Cell Biol.* 10:67. doi:10.1186/1471-2121-10-67

van der Wal, J., R. Habets, P. Várnai, T. Balla, and K. Jalink. 2001. Monitoring agonist-induced phospholipase C activation in live cells by fluorescence resonance energy transfer. *J. Biol. Chem.* 276:15337–15344. doi:10.1074/jbc.M007194200

Várnai, P., X. Lin, S.B. Lee, G. Tuymetova, T. Bondeva, A. Spät, S.G. Rhee, G. Hajnóczky, and T. Balla. 2002. Inositol lipid binding and membrane localization of isolated pleckstrin homology (PH) domains. Studies on the PH domains of phospholipase C delta 1 and p130. *J. Biol. Chem.* 277:27412–27422. doi:10.1074/jbc.M109672200

Villalba-Galea, C.A., W. Sandtner, D.M. Starace, and F. Bezanilla. 2008. S4-based voltage sensors have three major conformations. *Proc. Natl. Acad. Sci. USA.* 105:17600–17607. doi:10.1073/pnas.0807387105

Wang, Y.J., W.H. Li, J. Wang, K. Xu, P. Dong, X. Luo, and H.L. Yin. 2004. Critical role of PIP5KIγ87 in $InsP_3$-mediated Ca^{2+} signaling. *J. Cell Biol.* 167:1005–1010. doi:10.1083/jcb.200408008

Wenk, M.R., and P. De Camilli. 2004. Protein-lipid interactions and phosphoinositide metabolism in membrane traffic: insights from vesicle recycling in nerve terminals. *Proc. Natl. Acad. Sci. USA.* 101:8262–8269. doi:10.1073/pnas.0401874101

Willars, G.B., S.R. Nahorski, and R.A. Challiss. 1998. Differential regulation of muscarinic acetylcholine receptor-sensitive polyphosphoinositide pools and consequences for signaling in human neuroblastoma cells. *J. Biol. Chem.* 273:5037–5046. doi:10.1074/jbc.273.9.5037

Wilson, D.B., T.E. Bross, S.L. Hofmann, and P.W. Majerus. 1984. Hydrolysis of polyphosphoinositides by purified sheep seminal vesicle phospholipase C enzymes. *J. Biol. Chem.* 259:11718–11724.

Winks, J.S., S. Hughes, A.K. Filippov, L. Tatulian, F.C. Abogadie, D.A. Brown, and S.J. Marsh. 2005. Relationship between membrane phosphatidylinositol-4,5-bisphosphate and receptor-mediated inhibition of native neuronal M channels. *J. Neurosci.* 25:3400–3413. doi:10.1523/JNEUROSCI.3231-04.2005

Wirtz, K.W. 1997. Phospholipid transfer proteins revisited. *Biochem. J.* 324:353–360.

Xu, C., J. Watras, and L.M. Loew. 2003. Kinetic analysis of receptor-activated phosphoinositide turnover. *J. Cell Biol.* 161:779–791. doi:10.1083/jcb.200301070

Zaika, O., G.P. Tolstykh, D.B. Jaffe, and M.S. Shapiro. 2007. Inositol triphosphate-mediated Ca^{2+} signals direct purinergic P2Y receptor regulation of neuronal ion channels. *J. Neurosci.* 27:8914–8926. doi:10.1523/JNEUROSCI.1739-07.2007

Zaika, O., C.C. Hernandez, M. Bal, G.P. Tolstykh, and M.S. Shapiro. 2008. Determinants within the turret and pore-loop domains of KCNQ3 K^+ channels governing functional activity. *Biophys. J.* 95:5121–5137. doi:10.1529/biophysj.108.137604

Zhang, H., L.C. Craciun, T. Mirshahi, T. Rohács, C.M. Lopes, T. Jin, and D.E. Logothetis. 2003. PIP_2 activates KCNQ channels, and its hydrolysis underlies receptor-mediated inhibition of M currents. *Neuron.* 37:963–975. doi:10.1016/S0896-6273(03)00125-9

Zhao, X., P. Várnai, G. Tuymetova, A. Balla, Z.E. Tóth, C. Oker-Blom, J. Roder, A. Jeromin, and T. Balla. 2001. Interaction of neuronal calcium sensor-1 (NCS-1) with phosphatidylinositol 4-kinase β stimulates lipid kinase activity and affects membrane trafficking in COS-7 cells. *J. Biol. Chem.* 276:40183–40189.